The Influence of the Collagen Architecture on the Mechanical Response of the Human Cornea

Anna Pandolfi

Abstract The hierarchical architecture of the stromal collagen is strictly related to the optical function of the human cornea. The basic features of the corneal collagen organization have been known for a while, but recently the advance of optical imaging has revealed changes across the thickness that might be related to particular aspects of the corneal behavior. It is worth to investigate whether the actual structure possesses some relevance in the overall mechanical behavior of the cornea and whether it should not be disregarded in computational models with predictive purposes. In this study, finite element analyses of the human cornea considering four different architectures of the collagen are presented. Results of the numerical simulations of quasistatic and dynamic tests are compared and discussed.

1 Introduction

The corneal stroma plays several pivotal roles within the eye. Optically, the cornea is the main refracting lens and thus has to combine almost perfect transmission of visible light with precise shape, in order to focus incoming light. Furthermore, the cornea has to be extremely tough mechanically in order to protect the inner contents of the eye. These functions are governed by the corneal structure at all hierarchical levels. The evolution of modern refractive surgery has focused attention on the relationship between collagen architecture and biomechanical properties of the human cornea, in particular trying to establish factors that help in maintaining the corneal shape and transparency under physiological, pathological, or surgical conditions.

The corneal stroma transparency depends particularly on the regular ordering of stromal collagen fibrils, which cause destructive interference from scattered light except in the forward direction [1]. Collagen structural protein is characterized by triple helical domains, which self-assemble into fibrils that further form fibers and more complex three-dimensional networks responsible for the architecture of organs. The structural units of the stroma are the ribbon-like fibers called lamellae which

A. Pandolfi (✉)
Politecnico di Milano, Milan, Italy
e-mail: anna.pandolfi@polimi.it

E. Oñate et al. (eds.), *Advances in Computational Plasticity*, Computational Methods in Applied Sciences 46, DOI 10.1007/978-3-319-60885-3_16

consist of aligned, evenly spaced collagen fibrils surrounded by a proteoglycan-rich matrix. Stromal lamellae run parallel to the mean surface of the cornea shell, counting approximately 300 in the central cornea and 500 close to the limbus. This hierarchical organization of collagen is crucial to the biophysical and mechanical properties of the cornea.

Qualitative observations on the variation of collagen architecture through the depth of the human corneal stroma have been documented for over 100 years [2]. Kokott studied the organization of collagen bundles in human cornea and sclera by tearing their fibrils apart [3] and concluded that the lamellae had an orthogonal arrangement in the central cornea and extended without interruption from limbus to limbus, with a circular arrangement at the limbus itself. Earlier X-ray diffraction studies showed that about 49% of the stromal lamellae are preferentially aligned orthogonally, along the vertical and horizontal meridians [4]. Advanced imaging techniques, such as optical coherence tomography (OCT) and the second-harmonic generation imaging (SHG, a particular type of non-linear optical microscopy), have now provided new insights on the in-depth organization of the stromal collagen. Although such techniques are not yet applicable in-vivo to produce reliable patient-specific models, the recent findings may be of relevance in the optical and mechanical behavior of the cornea, and the actual architecture of the collagen should be considered in a numerical model with predictive ambitions.

The importance of the stromal microstructure has been acknowledged in several numerical models of the anterior chamber of the eye built with the aim of estimating the mechanical properties of the cornea or supporting surgical interventions [5, 6]. Indeed, the opportunity of recreating the exact microstructural and morphological features of the cornea is recognized in advanced model of artificial engineered tissues planned to be used in corneal transplants [7].

Aim of this study is to introduce the multiple features of the collagen architecture that OCT and SHG have revealed into an advanced numerical model of the cornea, and to ascertain the relevance of such microstructures on the mechanical response of the anterior chamber through the simulation of in-vivo static and dynamic tests.

2 Advanced Insights in Collagen Architecture of the Human Cornea

The basic principles of corneal structure and transparency have been known for some time, but in recent years X-ray scattering and other methods have revealed that the details of this structure are far more complex than previously thought and that the intricacy of the arrangement of the collagenous lamellae provides the shape and the mechanical properties of the tissue. Light microscopy was sufficient to discover more interweaving of lamellae in the anterior layers than the posterior, characterized by thinner lamellae that weave in and out of each other with orientations that are inclined relative to the corneal surface. The development of modern imaging techniques has led to improved quantification of lamellar size and organization.

The hypothesized structure hand drawn by Kokott [3] included the presence of superior–inferior (SI) and nasal–temporal (NT) preferred directions at the center of the cornea and circumferential directions at the limbus. With X-ray diffraction experiments, Meek et al. [8] first quantified the orientation of lamellae as viewed in the plane perpendicular to the optical axis. Scanning electron microscopy (SEM) and transmission electron microscopy (TEM) measurements demonstrated that posterior lamellae are one order wider and twice as thick as anterior lamellae [9]. SEM imaging was used to show how lamellae branch and interweave, and to quantify the in-plane angles between adjacent lamellae [10]. The raw X-ray data provide scattering intensities versus orientation on a discrete grid of points over the cornea surface corresponding to the experimental measurement procedure, but do not provide information about scattering variations with depth. X-ray diffraction combined with electron microscopy have shown that collagen lamellae in the posterior cornea are generally twice as thick as those in the anterior [9, 11]. Later studies proved the presence of aligned collagen running between adjacent cardinal points forming chords across the outer cornea [12]. These additional lamellae have been supposed to contribute to peripheral corneal flattening and seem to occur only in the posterior third of the cornea.

The regional differences in lamellar orientation across and throughout the thickness of the normal human cornea were analyzed in [13]. Collagen in the central 8 mm shows a strong orthogonal alignment, along the SI and NT directions, but only in deeper stromal regions. The average percentage of total fibers exhibiting the well-known preferred azimuthal directions was 42% in the posterior third thickness, but only 22% in the anterior third. This increase in alignment toward the posterior is quite interesting because it is in clear contrast with the trend of more inclined fibers toward the anterior. Another aspect of lamellar organization believed to be of mechanical importance is the interlamellar interaction as a result of interweaving [14]. Interlamellar sliding may be important for describing changes of the mechanical behavior with aging and the development of pathological situations such as keratoconus and ectasia after surgical intervention.

In the attempt of characterizing the elastic properties of the stromal tissue, Petsche et al. [15] found that the shear modulus is two to three orders of magnitude inferior to the tensile moduli, commonly measured and reported in the literature. They observed that the transverse shear stiffness of the cornea varies with the depth, and the shear stiffness of the anterior cornea is almost one order of magnitude greater than that the one of the posterior cornea. It was hypothesized that the inclination of lamellae in the anterior cornea and the decreasing degree of inclination with depth must be responsible for the measured depth dependent transverse shear properties, because the density of the collagen does not vary markedly with depth.

The well-documented limbal collagen annulus circumscribing the human cornea is located in the posterior third of the limbus thickness, according to the observations documented in [13], while the arrangement becomes less unidirectional in proximity to the anterior surface of the cornea. In addition to the contribution from the

dominant direction of fibril alignment, the different mechanical properties of the peripheral cornea and limbus with respect to the central tissue are influenced by the increment in both the size of the collagen fibrils and the number of lamellae [16].

Electron microscopy and X-ray scattering patterns obtained by using synchrotron radiation source have provided very important information about the anisotropic arrangements of collagen lamellae through the whole stroma in different regions of the cornea. Nevertheless, both techniques require tissue fixation preventing any in-vivo mechanical assays. More recently, SHG microscopy has proven to be an efficient tool for obtaining *virtual biopsies* in unstained fresh corneas, and introduce the viability of constructing patient-specific models.

To date, patient-specific models of the collagen architecture of the human cornea are not available and are not used directly in clinical applications, although advanced models that account for the details of the corneal collagen architecture have been around for a while [5, 6, 17–25]. Several investigations have pointed out that any material point within the cornea will have a unique lamellar orientation distribution; precise symmetry in the distributions over corneal quadrants is not observed in general, and realistic modeling cannot assume such symmetry. This is true especially when distributions associated with pathological conditions are modelled. Petsche and Pinsky [26] introduced a corneal model where the collagen orientation was taken directly from X-ray diffraction measurements on a single, full thickness, cornea. Incorporating the X-ray diffraction data describes the anisotropy resulting from the well documented SI and NT preferred directions of lamellae in the vicinity of the corneal vertex as well as the circumferentially preferred orientations at the limbus. The model in [26] included 3D lamella orientations and inclinations in the view to explain the depth-dependent shear stiffness properties and to fully characterize the mechanics of inclined lamellae. A microstructural model proposed in Studer et al. [27] first accounted for some interlamellar effects by including, in their formulation, ad hoc cross-link fibers perpendicular to the lamellar directions but without depth dependence.

Beside exhaustive information on the geometry of eye and on the microstructure of the stroma [28], a patient-specific numerical model of the cornea requires the realistic characterization of the mechanical properties of the materials [29]. Mechanical properties cannot be simply determined through optical imaging, but it is necessary to setup a protocol of in-vivo static and dynamic tests, thought and carried on in a concerted manner, to allow the identification of the material model. Tests must be combined with identification procedures based on inverse analysis, that, simulating the experimental tests, will provide the best estimate of the sought material properties.

An important question emerging in the definition of a numerical model of the cornea—a model obviously predictive in the view of applications in surgical practice—concerns the ability of a mechanical test to spring out the micromechanical characteristics of the cornea. In spite of several studies recently published, the mechanical consequences of specific collagen architectures have not been investigated sufficiently in the literature, especially in terms of overall configurations; in general only global averaged quantities are provided. Often, comparisons with in-

vivo experiments have been limited to a component of displacement, or a displacement profile [30, 31]; with a few exceptions [20, 32], no documentation of the stress level observed in the numerical simulations is reported, thus a comparison between the performance of different models is hardly possible.

In the following, we present a numerical study conducted with the aim of comparing the mechanical response of different collagen architectures in a model of human cornea undergoing in-vivo static and dynamic tests. For the sake of simplicity, we use a model of the cornea that we have been developing in-house, and consider a patient-specific geometry acquired with a corneal topographer and already used in previous studies [28, 31, 33].

3 Material and Methods

The finite element method has been widely used for modeling the behavior of the cornea, under static and dynamic conditions [6, 17, 19, 21–23, 25]. In the last decade we have been developing an ad-hoc finite element code [6, 20, 28, 32, 34] with the following distinguished features: (i) patient-specific geometries directly derived from corneal topographies; (ii) stochastic fiber distributed material models, to describe the complex architecture of reinforcing collagen fibrils in the stromal tissue; (iii) automatic identification of the stress-free configuration of the cornea; (iv) customization of the main material parameters of the cornea on the basis of diagnostic measurements.

3.1 Geometrical and Material Model

Patient-specific geometries of the cornea, constructed using an ad hoc software from sets of anterior and posterior corneal surface coordinates supplied by ocular topographer (Sirius, CSO, Italy) [28], are automatically discretized at the desired level of refinement in standard finite elements, e.g., 8-node bricks with linear interpolation of the displacements, see Fig. 1. The knowledge of the physiologic geometry of the cornea is not sufficient to create a patient-specific numerical model. The topographer images refer to the cornea reacting to the intraocular pressure (IOP) exerted by the filling gels. A correct stress analysis requires the recovery of the stress-free configuration, corresponding to a null IOP. The automatic procedure that allows for the recovery of the stress-free configuration is described in [28].

Necessarily, the model has several limitations. It accounts only for the main central layer (stroma) of the cornea and disregards the thin anterior and posterior membranes, known to provide negligible contributions to the mechanical stiffness of the cornea. The geometrical model does not include the adjacent biological tissues, i.e., the white sclera and the iris, which are accounted for in terms of compliant boundaries at the limbus [32]. Adjacent tissues are not included because of the lack of

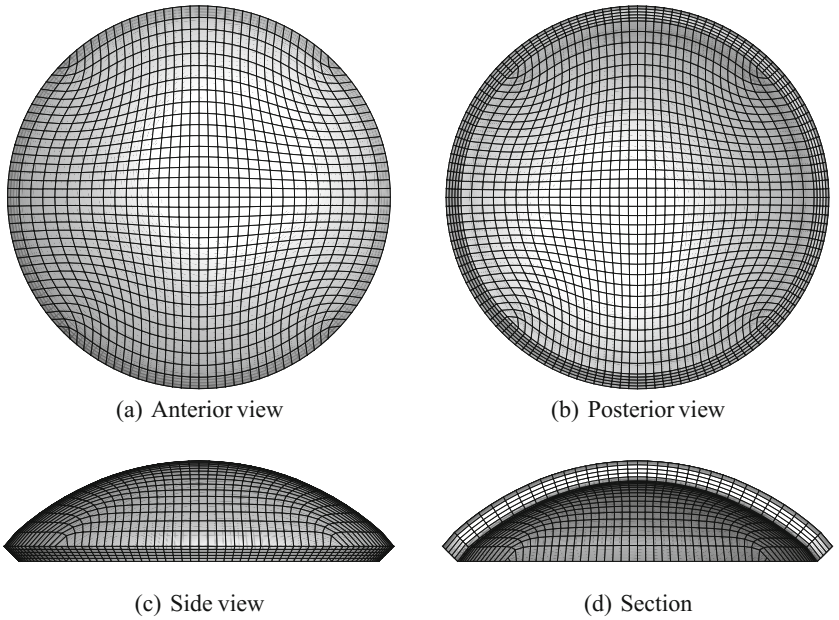

(a) Anterior view (b) Posterior view

(c) Side view (d) Section

Fig. 1 Patient specific finite element model of the cornea. The mesh comprises 7,350 nodes and 5,780 8-node elements. The geometry refers to the stress-free configuration of a corneal topography already used in previous studies [28], with a finer finite element discretization

knowledge of their in-vivo mechanical characteristics, to avoid uncertainties larger than the ones introduced by the exclusion of such parts. As explained in [20], a reasonable choice of the cornea boundary conditions narrows the effects of these deficiencies. Finally, the model does not account explicitly for the interaction between the deformable cornea and the ocular fluid (aqueous humor) filling the anterior chamber. Fluids may play a role in a dynamic test, because they interact with the posterior surface of the moving cornea. While we are currently developing a numerical algorithm of fluid-solid interaction to analyze the problem with more accuracy [35], we account here for the presence of the fluid in a simplified way, by adding extra masses to the posterior nodes of the discretized cornea, cf. [33].

The material model adopted for the stroma is hyperelastic and anisotropic, accounting for statistically distributed sets of collagen fibrils with a second order approximation, and able to switch from fully 3D [36] to planar [37] von Mises type distributions of the orientation of the fibrils, described by a coefficient b. In keeping with approaches typically adopted in the modelling of biomaterials, the behavior of the proteoglycan matrix and of the reinforcing collagen fibrils is modeled separately. Thus, the strain energy density function Ψ is assumed to be the sum of three independent contributions with full separation of the arguments:

$$\Psi = \Psi_{\text{vol}}(J) + \Psi_{\text{iso}}(\bar{I}_1, \bar{I}_2) + \Psi_{\text{aniso}}(I^*_{4M}). \tag{1}$$

The term Ψ_{vol} accounts for the volumetric elastic response and depends on the Jacobian $J = \det \mathbf{F}$, where $\mathbf{F} = \partial \mathbf{x}/\partial \mathbf{X}$ is the deformation gradient. Ψ_{vol} is regarded as a penalty term to enforce the incompressibility constraint and has the operative form

$$\Psi_{\text{vol}}(J) = \frac{1}{4} K (J^2 - 1 - 2 \log J), \tag{2}$$

where K is a stiffness coefficient related to the bulk modulus. The term Ψ_{iso} describes the behavior of the isotropic components of the material, and depends on the first and second invariants, $\bar{I}_1$ and $\bar{I}_2$ (see Appendix) of the isochoric Cauchy-Green deformation tensor $\overline{\mathbf{C}} = \overline{\mathbf{F}}^T \overline{\mathbf{F}}$, with $\overline{\mathbf{F}} = J^{-1/3}\mathbf{F}$, according to Mooney-Rivlin's model

$$\Psi_{\text{iso}}(\bar{I}_1, \bar{I}_2) = \frac{1}{2}\mu_1(\bar{I}_1 - 3) + \frac{1}{2}\mu_2(\bar{I}_2 - 3), \tag{3}$$

where $\mu = \mu_1 + \mu_2$ is the shear modulus of the material. The term Ψ_{aniso} addresses the anisotropic contribution of two statistically dispersed families of collagen fibrils. The M fibril family is defined in terms of a unit vector field, $\mathbf{a}_M(\mathbf{x})$, that identifies the dominant orientation of the fibrils, and by a dispersion coefficient $b(\mathbf{x})$, cf. [32]. The anisotropic strain energy function Ψ_{aniso} used in the model is

$$\Psi_{\text{aniso}}(I^*_{4M}, K^*_M) = \sum_{M=1}^{2} \frac{k_1}{2k_2} \exp\left[k_2 \left(I^*_{4M} - 1\right)^2\right] \left(1 + K^*_M \sigma^2_{I_4 M}\right), \tag{4}$$

where k_1 is a stiffness parameter for fibrils in moderate extension, and k_2 is a dimensionless rigidity parameter that describes the behavior of fibrils in large extension. The expression of the variables I^*_{4M} and K^*_M in Eq. (4), that describes the dispersion of the fibrils in both 3D and planar distribution, is reported in Appendix. The material model is characterized by five parameters: the bulk modulus K, two shear moduli μ_1 and μ_2 for the Mooney-Rivlin model, the fibril stiffness k_1, and the fibril rigidity k_2. The set of elastic material properties calibrated for the patient group in [28] is used also in the present study, see Table 1.

Here we restrict our attention to the collagen architecture of the cornea and to the way the different features recently pointed out by the research in the field are affecting the mechanical response of the cornea. The simulations illustrated here make use of a reference model (baseline) for the internal structure of the collagen fiber distribution, describing an architecture of the fibrils which is in line with X-ray imaging on ex-vivo corneas [12, 38], presenting different levels of the dispersion parameter $b(\mathbf{x})$ in different locations of the cornea. Fibrils are strongly aligned at the center, where they follow an orthogonal organization in the NT and SI directions; at the periphery fibrils are mostly aligned to the limbus circumference, see Fig. 2, cf. [28, 32]. In the baseline model, a fully 3D dispersion model of the fibrils is considered, with no variations across the thickness.

Table 1 Material parameters used in the present study, cf. [28]

Model	K [MPa]	μ_1 [MPa]	μ_2 [MPa]	k_1 [MPa]	k_2	b	ρ [kg/m^3]
Baseline	5.5	0.06	−0.01	0.04	200	0.2−2.8 (in plane)	1,062
ST	5.5	0.06	−0.01	0.0091−0.091	36−360	0.2−2.8 (in plane)	1,062
SL	5.5	0.06	−0.01	0.0091−0.091	36−360	0.2−2.8 (in plane)	1,062
DT	5.5	0.06	−0.01	0.04	200	0.2−2.8 (thickness)	1,062

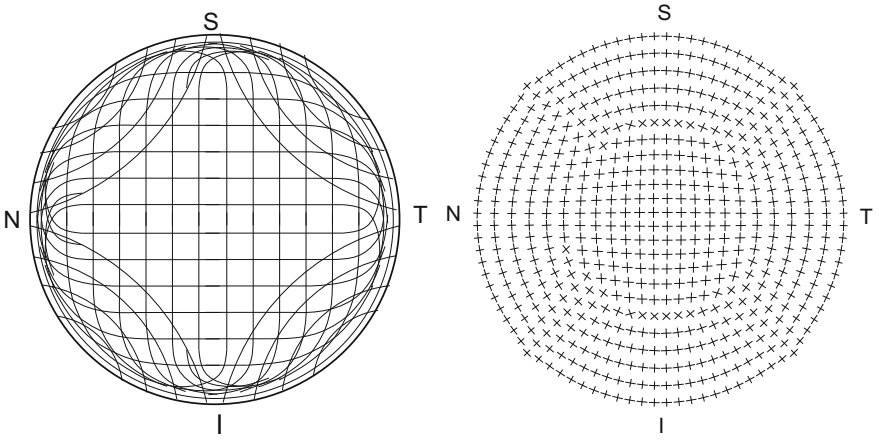

(a) X-ray structure (b) Fibrils main orientation

Fig. 2 **a** Structure of the fibril organization within the cornea, cf. [12, 38]. S denotes the superior point, I the inferior point, N the nasal point and T the temporal point. **b** Main orientation of the fibrils assumed in the numerical model. In the central region, the two sets of fibrils have an equivalent stiffness. In the limbial region, the two sets of fibers may have a different stiffness

In the numerical models considered in this comparative study, we preserve the orientation of the fibrils described in Fig. 2b, but include variations in the dispersion and in the stiffness of the two sets of fibers, in order to incorporate more recent findings and to evaluate their relevance on the global mechanical response of the cornea. We consider the following three alternative models:

1. Model ST. Variation of the stiffness across the thickness. The stiffness of the fibrils in the anterior stroma is set 10 times larger than the stiffness of the fibrils of the posterior stroma, according to the experimental observation reported in [15].
2. Model SL. Variation of the stiffness and of the dispersion of the fibrils at limbus. The dispersion of the fibrils at the limbus is varied from $b = 0.2$ on the anterior

surface to $b = 2.8$ in the posterior surface. Moreover, the stiffness parameters of the fibrils running circumferentially in the deepest one third of the limbal thickness are set 10 times larger than the stiffness parameters of the fibrils oriented radially, to follow the observation reported in [13].

3. Model DT. Variation of the dispersion of the fibrils across the thickness. We use a fully 3D von Mises dispersion model, assigning different values of the dispersion coefficient from the anterior ($b_{\min} = 0.2$) to the posterior ($b_{\max} = 2.8$) surface, as a simplified trial to reflect the indication reported in [39].

The range of the parameters used in the four model for the numerical analyses are listed in Table 1.

3.2 Static and Dynamic Analysis

In the view of future clinical applications, the comparison between the four different models is achieved through the simulation of two in-vivo mechanical contact and contactless tests. Mechanical tests induce an important deformation localized at the center of the cornea, without damaging its delicate tissues. Simulations require to conduct an initial static analysis, to attain a stress state corresponding to the condition of the cornea under the action of the physiological IOP, which in this calculation is set 16 mmHg = 2.13 kPa. The boundary conditions imposed to the nodes at the limbus allow for the rotation of the cornea about the limbus circumference, optimizing the difference between the current model and a model that includes limbus and sclera, see [20].

Once the physiological state has been reached, the static or dynamic test begins. For the static test, we model the action of an optomechanical testing device [40] which applies a mechanical probe at the corneal apex. The loading procedure consists in advancing the mechanical probe in six steps of 100 μm into the cornea. The probe is a 0.5 mm diameter cylindrical indenter with a hemispherical tip [15]. Static analysis are conducted with an explicit solver.

For the dynamic test, we model the action of a contactless ocular tonometer (CorVis ST) that induces a motion of the cornea with a localized air jet. The sudden pulse exerted by the instrument causes the inwards motion of the cornea, which passes through an applanation, and successively snaps into a slight concavity. When the air pulse pressure decreases, the elastic corneal tissue recovers the original configuration, passing through a second applanation. Although the actual space and time profile of the air jet pressure and its maximum value are not provided by the instrument, the imprint of the air jet on the anterior corneal surface has been estimated, through preliminary parametric analyses, using an analytical expression [31]. The air jet pressure is applied over a 1.5 mm radius circular area centered at the apex of the cornea. The pressure has the functional form

$$p(t,r) = p_0 \exp\left[-64\left(\frac{t}{T} - \frac{1}{4}\right)^2\right] \exp\left(-0.44r^2\right) \tag{5}$$

where $p_0 = 40$ kPa is the maximum air jet pressure, $T/2 = 20$ ms the duration of the air jet, and r the distance in mm from the center of the jet of a point on the corneal surface, cf. [31]. Note that the dynamical test is not correctly modelled, since the presence of the fluids filling the anterior chamber of the eye has been disregarded for the sake of simplicity. Since the effect of the fluid-structure interaction is not accounted for, the analysis is not able to describe the final part of the test, where a delay in the motion of the cornea is observed due to the presence of the fluid. As already mentioned, this issue is currently tackled in a parallel work [35]. The dynamical analysis is conducted with a central difference time stepping algorithm.

Prior to conduct the numerical tests, the stress-free configuration for the four models case has been identified through the iterative procedure described in [32]. The stress-free geometry has been used subsequently for the quasistatic and dynamic analysis.

Before conducting the simulation of the two in-vivo mechanical tests, we simulated an ideal inflation test, where the cornea is loaded with a growing IOP from 0 to 40 mmHg.

4 Results

Figure 3 shows the results of the ideal inflation test for the four models, in terms of IOP versus the displacement of the cornea apex. The curves superpose well to the baseline curve up to the physiological IOP (16 mmHg), revealing a maximum

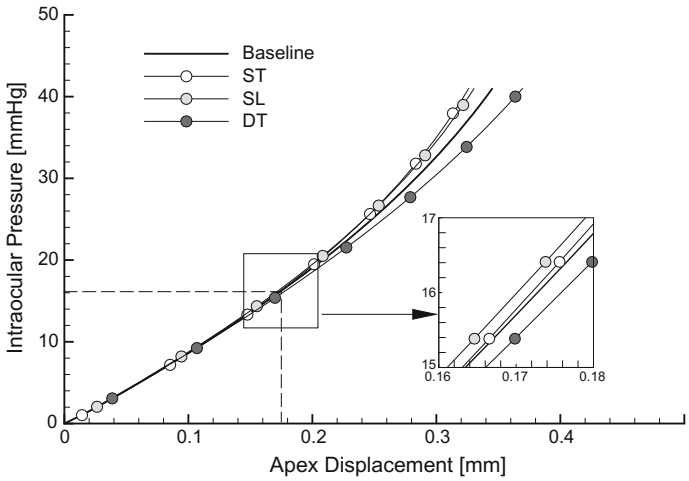

Fig. 3 Inflation test. Force applied to the probe versus apex displacement. The *thick line* represents the response of the reference model

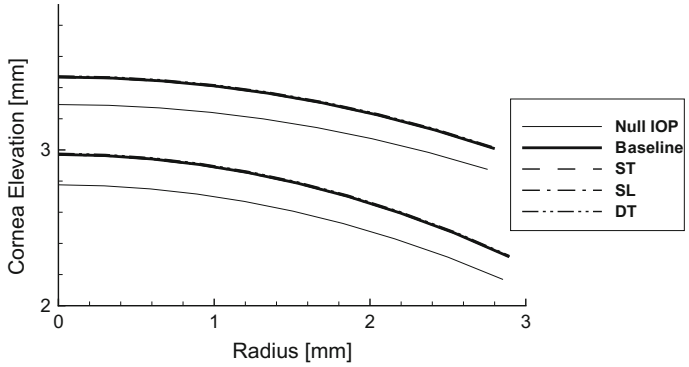

(a) NT meridian

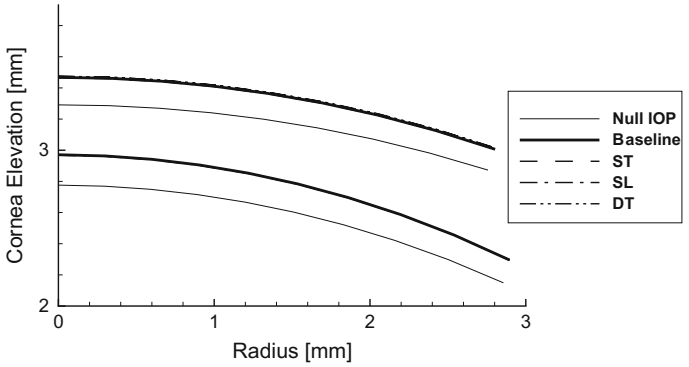

(b) SI meridian

Fig. 4 Inflation test. Comparison of the anterior and posterior profiles of the cornea at the physiological IOP, along the **a** Nasal-Temporal meridian (from center to Temporal side); **b** Superior-Inferior meridian (from the center of the cornea to the superior edge). *Thin lines* denote the posterior and anterior surfaces of the cornea at zero IOP

relative displacement less than 2 μm. The similarity of the response is further highlighted in Fig. 4, where the numerically computed corneal profiles along the NT and SI meridians are compared. Differences between the geometrical configurations associated to the four models cannot be appreciated. However, at higher IOP the four curves show marked differences, and are characterized by a stiffer response (ST and SL models) or a more compliant response (DT model) with respect to the baseline model, see Fig. 3.

The results of the simulations of quasistatic contact tests are shown in Figs. 5 and 6. Figure 5 compares the global mechanical response of the four models in terms of probe force versus probe displacement, which corresponds to the displacement of the corneal apex. In the whole range of the imposed displacements, the curves corresponding to the DT and SL models show a small deviation from the curve of the baseline model. In particular, the DT model reveals a more compliant behavior,

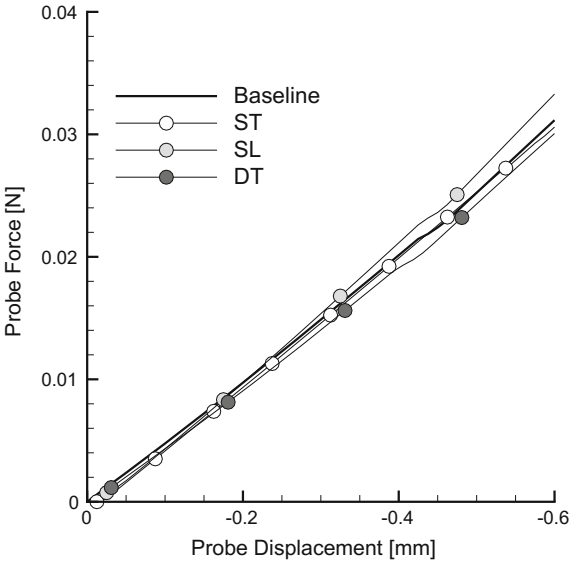

Fig. 5 Probe test. Cornea profiles at the maximum displacement of the probe, corresponding to an indentation of the cornea of 0.6 mm. The *dashed curves* represent the anterior and posterior surface of the cornea at the physiological IOP

requiring a smaller force to reach the final displacement of the probe. Contrariwise, the SL model is characterized by a stiffer behavior, with a larger force exerted by the probe. The ST model, instead, does not show marked differences with respect to the baseline model. The small differences in the mechanical response to the probe action can be appreciated in Fig. 6, where the corneal profiles along the NT and SI meridian obtained for the four models are visualized. The more compliant behavior of the DT model leads to an enhanced deformation in the peripheral zone at 2 mm from the corneal center; while the stiffer model SL shows a less marked deformation in the same area.

The results of the simulations of dynamic contactless tests are visualized in Figs. 7 and 8. Figure 7 compares the response of the four models considering the displacement of the corneal apex. Figure 7a shows the time history of the apex displacement for the four models. Figure 7b shows the mechanical response of the four models in terms of air jet pressure versus apex displacement. Unlikely the other tests previously discussed, dynamical tests highlight differences between the models. Figure 8 compares the configuration of the four models in correspondence to the maximum value of the applied air jet pressure. Note that the maximum displacement is reached at different times for the four models. The DT model is confirmed as the most compliant, showing a larger displacement at all times, while SL model confirms the stiffer behavior already shown in the other tests. The ST model, instead, behaves closely to the baseline model.

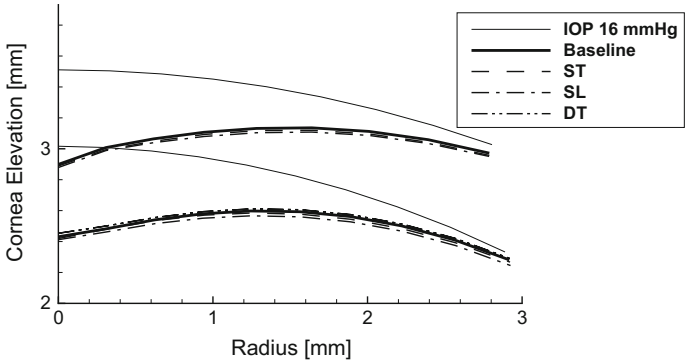

(a) NT meridian

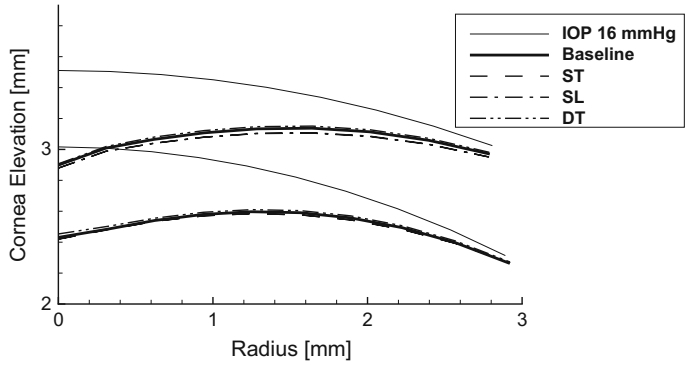

(b) SI meridian

Fig. 6 Probe test. Cornea profiles at the maximum displacement of the probe, corresponding to an indentation of the cornea of 0.6 mm. The *two thin lines* describe the anterior and posterior surfaces of the cornea at the physiological IOP

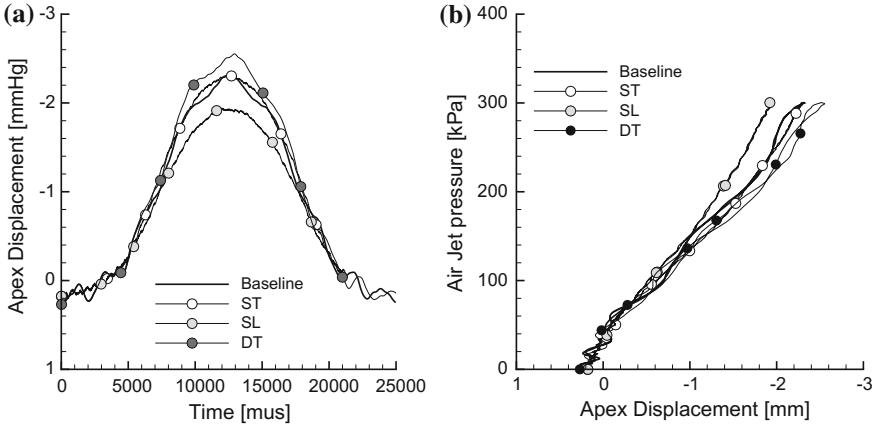

Fig. 7 Dynamic contactless test. **a** Cornea apex displacement time history. **b** Air jet pressure versus apex displacement curve. The *thick line* denotes the reference model

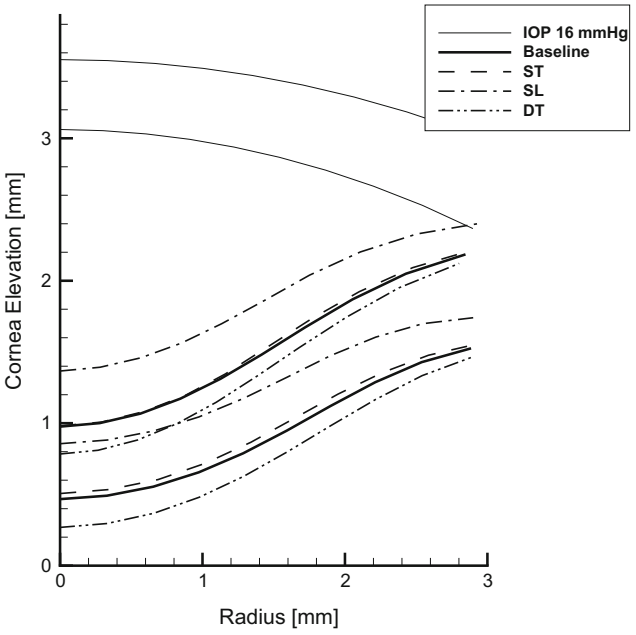

(a) NT meridian

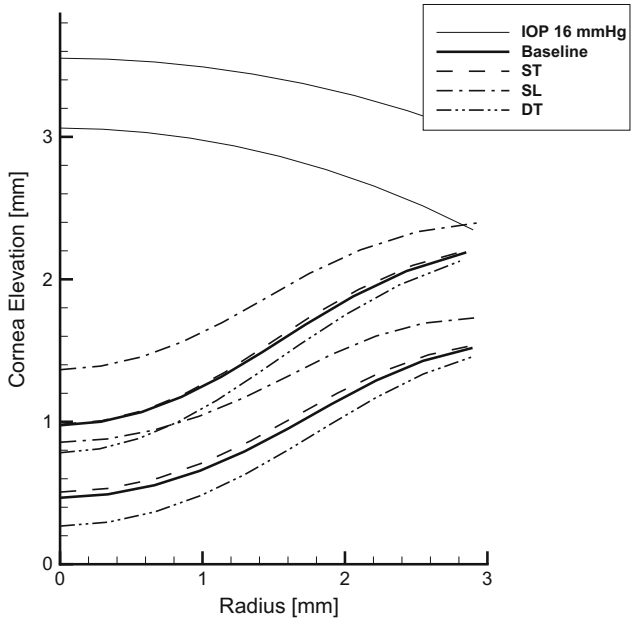

(b) SI meridian

Fig. 8 Dynamic contactless test. Comparison of the cornea profiles at the maximum value of the air jet for the four models. The *two thin line curves* represent the anterior and posterior surfaces of the cornea at the physiological IOP

5 Discussion and Conclusions

The description of the collagen architecture of the stroma in numerical models that are used to predict the biomechanical behavior of the human cornea has been object of a vibrant discussion in the last years. Modern diagnostic technologies and advanced optical instruments have provided accurate information about the organization of the collagen within the stroma thickness, although a definite physical or chemical motivation of such peculiar structure has not been found yet. Recent contributions in the literature have been presenting models of the human cornea that account for the variability of the collagen structure and distribution, see, e.g. [6, 28, 31–33, 41–45].

It is a commonly well accepted and acknowledged opinion that any predictive numerical model of the cornea, to be used to anticipate the outcomes of refractive surgery, must be personalized to the particular patient under consideration. This requires the identification of geometrical and material properties of the cornea by means of inverse procedures that compare the results of in-vivo tests with the outcomes of numerical simulations. However, given the nonlinearity of the models and the large kinematics involved in the tests, the identification procedures provide different values to the mechanical parameters of the cornea, according to the different material model adopted, see, e.g., [20]. The selection of the most appropriate material model, however, is not sufficient to ascertain the correct value of the material properties, because results may vary according to the model chosen to describe the underlining collagen structure of the stroma.

For a particular advanced hyperelastic, anisotropic, fiber dispersed based material model, here we study the response of a cornea model where the collagen microstructure within the stroma is assumed to vary in different manners across the thickness and at different locations of the surface. We refer to an advanced model of the human cornea used in recent works [28, 31, 32], evolution of the original model developed in [6, 34], and consider three variants, to account for the variability of the stiffness of the stroma across the thickness (ST model) or in proximity of the limbus (SL model), and for the different level of dispersion of the collagen across the thickness (DT model).

We begin by comparing the behavior of the four models considering an ideal inflation tests, where the cornea undergoes the action of a growing IOP. The inflation test is the most common simulation conducted in order to compare different material models, but this simple loading condition is not able to point out at all the differences between the models at the physiological IOP level, see Figs. 3 and 4. Moreover, the inflation test is all non-natural, it cannot be performed in-vivo, and thus cannot be used to characterize the mechanical properties of the cornea.

Next, we simulate a quasistatic mechanical test where a rigid probe, moved in small steps, indents the center of the cornea. Such a test, although not yet used routinely in clinical investigations, can be effectively used for the calibration of the material model of the cornea. The results of the probe test are able to visualize the differences between the four models. Numerical results seem to exclude

appreciable differences in the mechanical behavior between the baseline model and the SL model; while the ST and DT models present some difference in the displacement field.

Finally, we simulate the dynamical air puff test, commonly used in the modern clinical practice. The air jet acts at the center of the cornea for a very short time, and causes the inward deflection of the cornea in the central region. The mechanical response of the cornea models is visualized in Figs. 7 and 8. The apex experiences the larger displacements during the test, thus the plots in Fig. 7 clarify sufficiently the difference between the four models. The DT and ST models confirm their higher compliance and higher stiffness, respectively, while the SL model maintains a strong resemblance with the baseline model. The maximum deflected configurations of the four models are compared in Fig. 8. The differences between the SL model and the baseline model appear only in the profile plots, and, interestingly, involve mainly the posterior surface of the cornea.

In considering the results presented here, it is clear that simple inflation tests are not able to provide sufficient information about the material parameters that characterize the collagen structure of the cornea. In fact, the particular structure of the collagen is not activated by the test and the mechanical characterization of the parameters may lead to several sets of values. Contrariwise, in-vivo contact and contactless tests are able to activate (although in a non-natural manner) the particular internal structure of the reinforcing collagen, therefore they might be used to characterize a specific material model. Moreover, between the quasistatic and the dynamic tests, the air puff tests seems to be superior, in the sense that the amplitude of the induced displacements in the cornea might be easier to be measured through optical imaging.

According to the present study, it appears that the relevance of the collagen organization at the limbus is not very important in terms of mechanical response of the corneal shell. In fact, among the four models, the SL model is the closest to the baseline model in all the numerical simulations. This observation suggests that the main biomechanical features of the cornea derive from the structure of the collagen in the optical zone.

The present research has a few drawbacks that we are trying to remove in concurrent studies. The most important drawback, that affects only the dynamical tests, is the absence of the filling fluids, which indeed play an important role in the mechanical response of the system. We are presently developing a coupled fluid-structure interaction approach, based on meshfree discretazion of the fluid domain, to tackle this issue [35]. A second drawback is the missing comparison of the stress fields between the different models. The complexity of the stress fields induced by the contact and contactless tests requires a heavy manipulation of the numerical results, that are object of an additional current study.

Appendix

The first and second invariant of the isochoric Cauchy-Green deformation tensor are defined as

$$\bar{I}_1 = \mathrm{tr}\,\overline{\mathbf{C}}, \qquad \bar{I}_2 = \frac{1}{2}\left[(\mathrm{tr}\,\overline{\mathbf{C}})^2 - \mathrm{tr}(\overline{\mathbf{C}}^2)\right]. \tag{6}$$

The two pseudo-invariants $\bar{I}^*_{4M}, M = 1, 2$ are defined as

$$I^*_{4M} = \mathbf{H}_M : \mathbf{C}. \tag{7}$$

The structure tensor $\mathbf{H}_M$ is defined as

$$\mathbf{H}_M = \kappa_M \mathbf{I} + (1 - 3\kappa_M)\,\mathbf{A}_M, \qquad \mathbf{A}_M = \mathbf{a}_M \otimes \mathbf{a}_M, \tag{8}$$

$\mathbf{I}$ being the identity tensor. The scalar parameter κ_M depends of the chosen spatial distribution of the fibrils orientation $b_M(\mathbf{x})$. For 3D distributions characterized by rotational symmetry it holds [36]

$$\kappa_M = \frac{1}{4}\int_0^{\pi} \rho_M(\Theta)\sin^3\Theta d\Theta\,, \tag{9}$$

while for planar π-periodic distributions it holds [37]

$$\kappa_M^{\mathrm{pl}} = \frac{1}{\pi}\int_{-\pi/2}^{\pi/2} \rho(\Theta)\sin^2\Theta\, d\Theta\,. \tag{10}$$

The two terms

$$K^*_M = k_{2M} + 2\,k_{2M}^2\,\left(I^*_{4M} - 1\right)^2 \tag{11}$$

and

$$\sigma^2_{I_{4M}} / = \mathbf{C} : \langle \mathbf{A}_M \otimes \mathbf{A}_M \rangle : \mathbf{C} - \left(\mathbf{H}_M : \mathbf{C}\right)^2, \tag{12}$$

are introduced to include the variance of the fibril orientation distribution in the material model, see [36].

References

1. A.J. Bron, The architecture of the corneal stroma. Br. J. Ophthalmol. **85**(4), 379–381 (2001)
2. M. Salzmann, in *The Anatomy and Histology of the Human Eyeball in the Normal State, its Development and Senescence*, (University of Chicago Press, 1912)
3. W. Kokott, über mechanisch-funktionelle strukturen des auges. Albrecht von Graves Archiv für Ophthalmologie **138**(4), 424–485 (1938)

4. A. Daxer, P. Fratzl, Collagen fibril orientation in the human corneal stroma and its implication in keratoconus. Investig. Ophthalmol. Vis. Sci. **38**, 121–129 (1997)
5. P.M. Pinsky, D. van der Heide, D. Chernyak, Computational modeling of mechanical anisotropy in the cornea and sclera. J. Cataract Refract. Surg. **31**(1), 136–145 (2005)
6. A. Pandolfi, F. Manganiello, A material model for the human cornea. Constitutive behavior and numerical analysis. Biomech. Model. Mechanobiol. **5**, 237–246 (2006)
7. C.J. Connon, Approaches to corneal tissue engineering: top-down or bottom-up? **110**, 15–20 (2015)
8. K.M. Meek, T. Blamires, G.F. Elliot, T.J. Gyi, C. Nave, The organization of collagen fibrils in the human corneal stroma: a synchroton x-ray diffraction study. Curr. Eye Res. **6**, 841–846 (1987)
9. Y. Komai, T. Ushiki, The three-dimensional organization of collagen fibrils in the human cornea and sclera. Investig. Ophthalmol. Vis. Sci. **32**(8), 2244 (1991)
10. W. Radner, M. Zehetmayer, R. Aufreiter, R. Mallinger, Interlacing and cross-angle distribution of collagen lamellae in the human cornea. Cornea **17**(5), 537–543 (1998)
11. A.J. Quantock, C. Boote, R.D. Young, S. Hayes, H. Tanioka, S. Kawasaki, N. Ohta, T. Iida, N. Yagi, S. Kinoshita, K.M. Meek, Small-angle fibre diffraction studies of corneal matrix structure: a depth-profiled investigation of the human eye-bank cornea. J. Appl. Crystallogr. **40**(SUPPL.1), s335–s340 (2007)
12. H. Aghamohammadzadeh, R.H. Newton, K.M. Meek, X-ray scattering used to map the preferred collagen orientation in the human cornea and limbus. Structure **12**(2), 249–256 (2004)
13. M. Abahussin, S. Hayes, N.E.K. Cartwright, C.S. Kamma-Lorger, Y. Khan, J. Marshall, K.M. Meek, 3d collagen orientation study of the human cornea using x-ray diffraction and femtosecond laser technology. Investig. Ophthalmol. Vis. Sci. **50**(11), 5159–5164 (2009)
14. G. Wollensak, E. Sprl, C. Mazzotta, T. Kalinski, S. Sel, Interlamellar cohesion after corneal crosslinking using riboflavin and ultraviolet a light. Br. J. Ophthalmol. **95**(6), 876–880 (2011)
15. S.J. Petsche, D. Chernyak, J. Martiz, M.E. Levenston, P.M. Pinsky, Depth-dependent transverse shear properties of the human corneal stroma. Investig. Ophthalmol. Vis. Sci. **53**(2), 873 (2012)
16. C.S. Kamma-Lorger, C. Boote, S. Hayes, J. Moger, M. Burghammer, C. Knupp, A.J. Quantock, T. Sorensen, E. Di Cola, N. White, R.D. Young, K.M. Meek, Collagen and mature elastic fibre organisation as a function of depth in the human cornea and limbus. J. Struct. Biol. **169**(3), 424–430 (2010)
17. P.M. Pinsky, D. van Der Heide, D. Chernyak, Computational modeling of mechanical anisotropy in the cornea and sclera. J. Cataract Refract. Surg. **31**(1), 136–145 (2005)
18. D. Cabrera Fernández, A.M. Niazi, R.M. Kurtz, J.P. Djotyan, T. Juhasz, Finite element analysis applied to cornea reshaping. J. Biomed. Opt. **10**(6), 064018 (2005)
19. V. Alastrué, B. Calvo, E. Peña, M. Doblaré, Biomechanical modeling of refractive corneal surgery. J. Biomech. Eng. **128**, 150–160 (2006)
20. A. Pandolfi, G.A. Holzapfel, Three-dimensional modelling and computational analysis of the human cornea considering distributed collagen fiber orientation. J. Biomech. Eng. **130**, 061006 (2008)
21. E. Lanchares, B. Calvo, J.A. Cristbal, M. Doblar, Finite element simulation of arcuates for astigmatism correction. J. Biomech. **41**(4), 797–805 (2008)
22. A. Elsheikh, Finite element modeling of corneal biomechanical behavior. J. Refract. Surg. **26**(4), 289–300 (2010)
23. R. Grytz, G. Meschke, A computational remodeling approach to predict the physiological architecture of the collagen fibril network in corneo-scleral shells. Biomech. Model. Mechanobiol. **9**(2), 225–235 (2010)
24. A.S. Roy, W.J. Dupps, Patient-specific modeling of corneal refractive surgery outcomes and inverse estimation of elastic property changes. J. Biomech. Eng. **133**(1) (2010)
25. A.S. Roy, W.J. Dupps Jr., Patient-specific computational modeling of keratoconus progression and differential responses to collagen cross-linking. Investig. Ophthalmol. Vis. Sci. **52**(12), 9174–9187 (2011)

26. S.J. Petsche, P.M. Pinsky, The role of 3d collagen organization in stromal elasticity: a model based on x-ray diffraction data and second harmonic-generated images. Biomech. Model. Mechanobiol. **12**(6), 1101–1113 (2013)
27. H. Studer, X. Larrea, H. Riedwyl, P. Bchler, Biomechanical model of human cornea based on stromal microstructure. J. Biomech. **43**(5), 836–842 (2010)
28. I. Simonini, A. Pandolfi, Customized finite element modelling of the human cornea. PloS One **10**(6), e0130426 (2015)
29. A. Sinha Roy, K.M. Rocha, J.B. Randleman, R.D. Stulting, W.J. Dupps, Inverse computational analysis of in-vivo corneal elastic modulus change after collagen crosslinking for keratoconus. Exp. Eye Res. **113**, 92–104 (2013)
30. M.A. Ariza-Gracia, J.F. Zurita, D.P. Piñero, J.F. Rodriques-Matas, B. Calvo, Coupled biomechanical response of the cornea assessed by non-contact tonometry. A simulation study. PLoS One **10**(3), e0121486 (2015)
31. I. Simonini, M. Angelillo, A. Pandolfi, Theoretical and numerical analysis of the corneal air puff test. J. Mech. Phys. Solid **93**, 118–134 (2016)
32. P. Sánchez, K. Moutsouris, A. Pandolfi, Biomechanical and optical behavior of human corneas before and after photorefractive keratectomy. J. Cataract Refract. Surg. **40**(6), 905–917 (2014)
33. I. Simonini, A. Pandolfi, The influence of intraocular pressure and air jet pressure on corneal contactless tonometry tests. J. Mech. Beh. Biomed. Mater. **58**, 75–89 (2016)
34. A. Pandolfi, G. Fotia, F. Manganiello, Finite element simulations of laser refractive corneal surgery. Eng. Comput. **25**(1), 15–24 (2009)
35. A. Montanino, M. Angelillo, A. Pandolfi, Modeling the air puff test in the human cornea with a meshfree fluid-structure interaction approach 1–23 (2017, under review)
36. A. Pandolfi, M. Vasta, Fiber distributed hyperelastic modeling of biological tissues. Mech. Mater. **44**, 151–162 (2012)
37. M. Vasta, A. Gizzi, A. Pandolfi, On three- and two-dimensional fiber distributed models of biological tissues. Probab. Eng. Mech. **37**, 170–179 (2014)
38. K.M. Meek, C. Boote, The use of X-ray scattering techniques to quantify the orientation and distribution of collagen in the corneal stroma. Prog. Retinal Eye Res **28**(5), 369–392 (2009)
39. X. Cheng, P.M. Pinsky, Mechanisms of self-organization for the collagen fibril lattice in the human cornea. J. R. Soc. Interface **10**(87) (2013)
40. S.S. Chang, J.O. Hjortdal, D.M. Maurice, P.M. Pinsky, Corneal deformation by indentation and applanation forces. Investig. Ophthalmol. Vis. Sci. **34**, 1241 (1993)
41. A. Elsheikh, C. Whitford, R. Hamarashid, W. Kassem, A. Joda, P. Büchler, Stress free configuration of the human eye. Med. Eng. Phys. **35**(2), 211–216 (2013)
42. H.P. Studer, H. Riedwyl, C.A. Amstutz, J.V.M. Hanson, P. Bchler, Patient-specific finite-element simulation of the human cornea: a clinical validation study on cataract surgery. J. Biomech. **46**(4), 751–758 (2013)
43. C. Whitford, H. Studer, C. Boote, K.M. Meek, A. Elsheikh, Biomechanical model of the human cornea: considering shear stiffness and regional variation of collagen anisotropy and density. J. Mech. Behav. Biomed. Mater. **42**, 76–87 (2015)
44. A. Sinha Roy, M. Kurian, H. Matalia, R. Shetty, Air-puff associated quantification of non-linear biomechanical properties of the human cornea in vivo. J. Mech. Behav. Biomed. Mater. **48**, 173–182 (2015)
45. M.Á. Ariza-Gracia, S. Redondo, D. Piñero Llorens, B. Calvo, J.F. Rodriguez Matas, A predictive tool for determining patient-specific mechanical properties of human corneal tissue. Comput. Method Appl. Mech. Eng. **317**, 226–247 (2017)